ACS APPLIED MATERIALS & INTERFACES

Research Article

www.acsami.org

Origin of High Photocatalytic Properties in the Mixed-Phase TiO_2: A First-Principles Theoretical Study

Ming-Gang Ju,[†] Guangxu Sun,[†] Jiajun Wang,[†] Qiangqiang Meng,[†] and WanZhen Liang*[,‡]

[†]Department of Chemical Physics, University of Science and Technology of China, Hefei 230026, People's Republic of China

[‡]State Key Laboratory of Physical Chemistry of Solid Surfaces, Collaborative Innovation Center of Chemistry for Energy Materials, and Department of Chemistry, College of Chemistry and Chemical Engineering, Xiamen University, Xiamen 361005, People's Republic of China

ABSTRACT: We present a step-by-step theoretical protocol based on the first-principles methods to reveal the insight into the origin of the high photocatalytic activity achieved by the mixed-phase TiO_2, consisting of anatase and rutile. The interfacial geometries, density of states, charge densities, optical absorption spectrum, electrostatic potential, and band offsets have been calculated. The most stable mixed-phase structures have been identified, the interfacial tensile strain-dependent electronic structures have been observed, and the energy level diagram of band alignment has been given. We find that the geometrical reconstruction around the interfacial area has a negligible influence on the light absorption of the heterojunction and the interfacial sites seem not to dominantly contribute to the band-edge states. For the most stable heterojunction, the calculated valence-band maximum and conduction-band minimum of rutile, respectively, lie 0.52 and 0.22 eV above those of anatase, which agrees well with the experimental measurements and other theoretical predications. The good match of band energies to reaction requirements, large driving force for the charge immigration across the interface, and the difference of electrostatic potentials around the interface successfully explain the high photocatalytic activity achieved by the mixed-phase TiO_2.

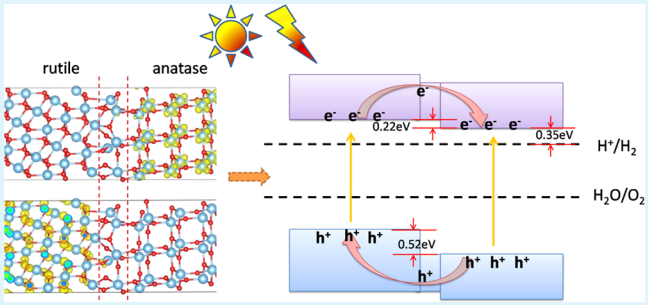

KEYWORDS: *mixed-phase TiO_2, band alignment, interfacial geometries, electronic properties, band offsets, separation of photogenerated carrier*

I. INTRODUCTION

The discovery of the photolysis of water on the surface of TiO_2 by Fujishima and Honda in 1972 has launched four decades of intensive research into the underlying chemical and physical processes involved.[1] TiO_2 has been widely studied as one of the most promising semiconductor photocatalysts for its various applications in photocatalysis and photoelectrochemistry due to its superior photocatalytic activity, chemical stability, low cost, and nontoxicity.[2−12] It is now clear that the photocatalytic performance of TiO_2 is strongly sensitive to its crystalline form. Two major crystalline phases of TiO_2 commonly used in photocatalytic reactions are anatase and rutile with a band gap of 3.2 and 3.0 eV, respectively.[13,14] Anatase is generally regarded as the more photochemically active than rutile due to its lower rates of recombination and higher surface absorptive capacity.[15]

Recent investigations have been focused on the mixed-phase TiO_2 materials because they have been demonstrated to exhibit higher activity than either single-phase.[16−24] To explain the synergetic effect between anatase and rutile, several efforts have been carried out.[25−30] Now, it is widely recognized that the high photocatalytic activity of mixed-phase TiO_2 materials is because the photogenerated charge carriers can be driven to the different phases by the band bending, and subsequently, the oxidation and reduction reaction sites are spatially separated.[16,17,31−34] However, there are some disputes and disagreements in the direction of interfacial charge transfer, energy band alignment, and the role of the interfacial sites on the interfacial electron transfer. Conventionally, it was thought that the anatase is the active component in mixed-phase TiO_2 with rutile serving passively as an electron sink due to the higher activity of the pure anatase phase than the rutile phase. The experiments on the electron paramagnetic resonance (EPR) spectroscopy[16] did not support that conclusion and showed that the photoinduced electrons actually transfer from the rutile to anatase. This observation was explained by the lower energy trap states in the anatase caused by the distorted interfacial sites, and these sites were further proposed as catalytically reactive hot spots.[16] A later experiment[35] alternatively concluded that mixed-phase materials have no significantly different activity in phase composition and specific surface area, but the photocatalytic activity is dominantly determined by the interconnection between anatase and rutile particles: the greater the interconnection, the greater the photocatalytic

Received: May 8, 2014
Accepted: June 25, 2014
Published: June 25, 2014

activity. Recently, several groups[31,33,34] have experimentally and theoretically proposed an opposite energy band alignment in mixed-phase TiO_2. They found that both the valence- and conduction-band edges of rutile located higher in energy level than those of anatase. Because of the higher valence-band maximum (VBM) and conduction-band minimum (CBM) of rutile, photogenerated electrons preferentially move from rutile to anatase and holes from anatase to rutile. This kind of band alignment explains the direction of charge transfer observed by EPR experiments[16,17] but may call into question about the assumption of the roles of low energy anatase trapping sites played on the charge transfer across the interface. It, therefore, requires an additional theoretical investigation on the microscopic atomic-scale geometrical features of the interface and their effects on the electronic properties of the junction.

The objectives of this paper are, therefore, two-fold. One is to shed light on details about the interfacial geometries. We will show how the atomic rearrangement in the interfacial area occurs when the materials of two different phases are brought together, how the atomic rearrangement affects the structural stability and electronic properties, and whether the interfacial sites dominantly contribute to the band-edge states of mixed-phase junctions. Another objective is to give a detailed knowledge about the electronic properties of the heterostructures and to further demonstrate the insight into the higher photocatalytic activity achieved by a mixed-phase junction. These properties are revealed via the calculations of total density of states (DOS), partial DOS (PDOS) yielded by projecting the total DOS onto the individual constituents of heterostructures, the optical absorption spectra, charge densities and the band offsets, etc. In particular, we investigate how the energy bands are affected by the tensile strain of the interfaces. The band offset, which describes the relative position of energy levels on both sides of the interface,[36] is one of the most important quantities to characterize an interface with such a staggered energy band alignment and a key parameter for tuning the carrier transport across a junction.[22,31,34,37] The valence-band offset (VBO) has been thus measured by X-ray photoelectron spectroscopy and calculated by density functional theory (DFT).[31,33,34] The conduction-band offset (CBO) has also been calculated, and a value of 0.24 eV is obtained.[31] In this work, both VBO and CBO are directly evaluated by the potential-line-up method[38−40] to provide further evidence for a staggered energy band alignment at the anatase and rutile interface. Meanwhile, we will investigate the localized DOS of different atomic layers along the junction to elucidate the effect of interfacial sites on the photocatalytic activity of the mixed-phase junction. Usually, the photocatalytic activity of the heterogeneous materials is largely related to the interfacial sites of the materials.

The paper is organized as follows: Section II briefly introduces the theoretical methods and the computational details. In section III, the calculated results are presented and analyzed. Finally, a concluding remark is given in section IV.

II. COMPUTATIONAL DETAILS

The first-principles calculations are performed using the projected augmented wave (PAW) plane-wave basis, implemented in the Vienna Ab initio Simulation Package (VASP).[41−43] An energy cutoff of 400 eV is employed, and the atomic positions are optimized using a conjugate gradient scheme without any symmetric restrictions until the maximum force on the each of them is less than 0.02 eV $Å^{-1}$. The pure-phase anatase and rutile are modeled with $8 \times 8 \times 4$ and $8 \times 8 \times 10$ grids for the k-point sampling, respectively. The mixed-phase heterostructures are modeled with a $4 \times 2 \times 1$ grid for the k-point sampling. The generalized gradient approximation (GGA) DFT exchange-correlation (XC) functional Perdew−Burke−Ernzerhof (PBE)[43] is employed for the geometrical optimization and the calculations of density of states (DOS) for all the heterostructures. A more accurate hybrid DFT XC functional HSE06[44,45] presented by Heyd, Scuseria, and Ernzerhof is adopted to perform the electronic-structure calculations for the most stable heterostructure. The hybrid functional HSE06 includes a fraction α of the screened short-range HF exchange to improve the derivative discontinuity of the Kohn−Sham potential for integer electron numbers. The default value of α in HSE06 is set to be 0.25. In the study, we set $\alpha = 0.21$ since we find that this value can yield exact agreement between the computed and experimental direct band gaps for both the pure-phase anatase and rutile.

In the investigation of the mixed-phase heterostructures, the periodically repeated supercells are used to keep the translational symmetry, in which two interfaces with the equivalence in terms of stoichiometry and geometry are involved in order to avoid electric fields due to unbalanced charges, and the adjacent interfaces are sufficiently separated to well present the isolated interface configuration. The charge depletion layer in the interface is revealed by the average electrostatic potential technique.[46] In this approach, the original space-dependent electrostatic potential $V(\vec{r})$ can be calculated by solving the Poisson equation based on the electron density given by the DFT calculations. The plane-averaged potential $\overline{V}(z)$ across the interface is obtained by

$$\overline{V}(z) = \frac{1}{S}\int_S V(\vec{r})\,\mathrm{d}x\,\mathrm{d}y \tag{1}$$

where S represents the area of a unit cell in the plane parallel to the xy plane. The bulklike oscillations in the $\overline{V}(z')$ with respect to the z coordinate in two phases can be further suppressed by the macroscopic average potential $\overline{\overline{V}}(z)$, which is given by

$$\overline{\overline{V}}(z) = \frac{1}{L}\int_{z-L/2}^{z+L/2} \overline{V}(z')\,\mathrm{d}z' \tag{2}$$

where L is the oscillation period of $\overline{V}(z')$.

On the basis of the macroscopic average $\overline{\overline{V}}(z)$, the band offsets of the mixed-phase junctions can be further performed.[37−40] The valence-band offset ΔE_{VBO} is given by

$$\Delta E_{VBO} = \overline{\overline{V}}_{mixed} + (E_{VBM} - \overline{\overline{V}})_{ana} - (E_{VBM} - \overline{\overline{V}})_{rut} \tag{3}$$

where $\Delta\overline{\overline{V}}_{mixed}$ represents the difference of $\overline{\overline{V}}(z)$ between two components in the mixed-phase junction, and the last two terms represent the difference between VBM energy (E_{VBM}) and $\overline{\overline{V}}(z)$ of the corresponding isolated component in the model. The similar strategy can be used for the calculation of ΔE_{CBO}.

III. RESULTS AND DISCUSSION

A. DOS Spectra of Pure-Phase Anatase and Rutile. To access the accuracy of different DFT XC functionals on the electronic structures of bulk materials, we calculate the DOS spectra of the pure-phase anatase and rutile by different DFT XC functionals. Figure 1 shows the calculated results. Explicitly, PBE underestimates the band gaps of both anatase and rutile. However, it provides the correct band gap difference of the two materials, which agrees exactly with the experimental value of 0.2 eV. DFT+U provides the accurate band gap for anatase, but a calculated band gap of 2.7 eV for rutile is lower than the experimental value of 3.0 eV.[13] Clearly, the experimentally measured band gaps of 3.2 and 3.0 eV for anatase and rutile are exactly yielded by the hybrid functional HSE06. However, the calculations with HSE06 are computationally expensive. We

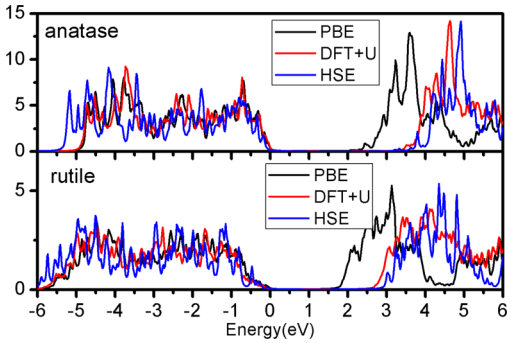

Figure 1. Total DOS of pure-phase anatase and rutile by PBE, DFT +*U*, and HSE06.

will, therefore, apply PBE for the geometrical optimizations and the calculations of DOS spectra for all the heterostructures and only apply HSE06 to calculate the electronic properties of the stablest heterostructure.

B. Interfacial Atomic Configurations of Mixed-Phase TiO_2. The local structures of surface and interfacial sites are critical for photocatalytic processes since these sites were thought to be the loci of the transfer and subsequent trapping of photogenerated charge carriers. At first, we, therefore, investigate the interfacial geometrical structures and the structure−property relationships of heterogeneous materials. The interfaces will be represented here by periodically alternating slabs of two phases. To construct the interfaces, one should follow the fundamental condition that the interface model should be electrically neutral and stoichiometric.[47] The mixed-phase junction between anatase and rutile is composed of well-matched lattice fringes between the (101) plane of anatase and the (111) plane of rutile, which has been indicated by the previous experimental work.[48] To identify possible stacking at the interface, we analyze the atomic-layer stacking of the (101) plane of anatase and the (111) plane of rutile. It is found that there are two different terminations possible, cleaved along the (101) plane of anatase and the (111) plane of rutile, respectively, as shown in Figure 2. The two different terminations of anatase are referred to as A1 and A2, and those of rutile are referred to as R1 and R2. They all maintain stoichiometry. The (101) plane of anatase has a surface cell size of 5.44 Å × 3.77 Å with ϕ = 110.3°, and the (111) plane of rutile has a surface cell size of 5.46 Å × 5.46 Å with ϕ = 107°. For the minimum in-plane lattice mismatch between the anatase (101) and rutile (111), we have considered a 1 × 3 surface supercell (corresponding to a surface supercell size of 5.44 Å × 11.3 Å with ϕ = 110.3°) for anatase and a 1 × 2 surface supercell (corresponding to a surface supercell size of 5.46 Å × 10.9 Å with ϕ = 107°) for rutile, respectively. Since each termination of anatase can, in principle, be combined with any terminations of rutile, there are four possible variances of the interfaces.[49] In our study, we denote these four different interfaces as A1−R1, A1−R2, A2−R1, and A2-R2. To keep the computational cost low, we only choose three interior angles (107, 108.7, and 110.3°) of surface supercells to construct the interface models of the mixed-phase TiO_2. In order to maintain the volume of supercells the same, the surface supercells of anatase and rutile are compressed and expanded about 1%, respectively. The models have 5 + 7 layers of surfaces of two phases, which can mimic the interface by our calculations, in principle, and the total content of the interface supercell model is $Ti_{60}O_{120}$.

The four relaxed heterostructure configurations are shown in Figure 3. From the optimized geometries, we find that the rutile phase around the interface of A1−R1 has an obvious reconstruction in the course of structural relaxation. The obvious reconstruction around the interfaces of A1−R2 and A2−R1 are not observed. A1−R2 possesses much poorer coordination in the interfacial area than A2−R1, and two different phase materials in A1−R2 are, therefore, weakly bonded. The structure A2−R2 combined with two less stable terminations of anatase (101) and rutile (111) has a complicated interface, and more reconstructions are observed in the course of structural relaxation. The relative stability of an interface is reflected by its formation energy. The lower the interfacial formation energy, the more stable the interface structure. For a repeated slab model, the interfacial formation energy can be expressed as[50−52] $E_{form} = (1/(2A))(E_{total} - nE_{ana} - mE_{rut})$, where E_{total} is the total energy of the slab supercell, and n and m are the numbers of TiO_2 units of the different phase components in the supercell, respectively. A denotes the interface cell area, and E_{ana} and E_{rut} denote the total energies per formula unit of bulk anatase and rutile, respectively. Figure 4 shows the calculated interfacial formation energies of the four types of junctions with different interior angles ϕ of surface supercells. The most stable structure is A2−R1 with ϕ = 108.7°. In contrast, the structure A2−R2 shows less stability. The structures A1−R1 and A1−R2 are slightly unstable configurations compared with A2−R1. In the following calculations, we mainly focus on the stable heterostructures formed by the A2−R1 interface.

C. Structure−Property Relationship of the Most Stable Mixed-Phase Heterostructures. First, the heterostructures A2−R1 with three different interior angles (107, 108.7, and 110.3°) of the surface supercell are optimized by maintaining the volumes of supercells. Then, their DOS and PDOS are calculated. The variation of DOS and PDOS via the interior angles is displayed in Figure 5, which reveals the structure−property relationship and the role of the strain around the interface played on the electronic properties. Compared with the total DOS of pure-phase anatase and rutile,

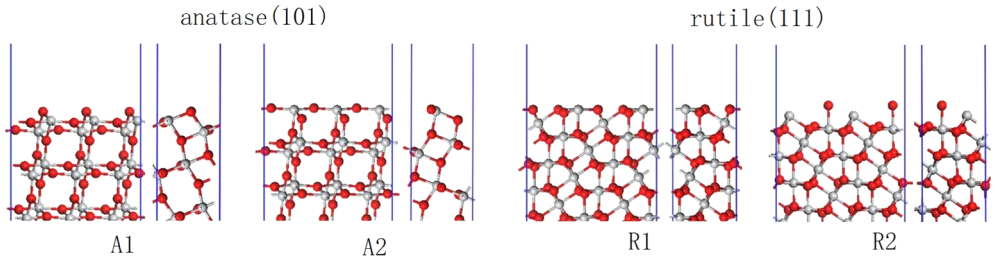

Figure 2. Different terminations of the (110) plane of rutile and the (101) plane of anatase (front view and side view).

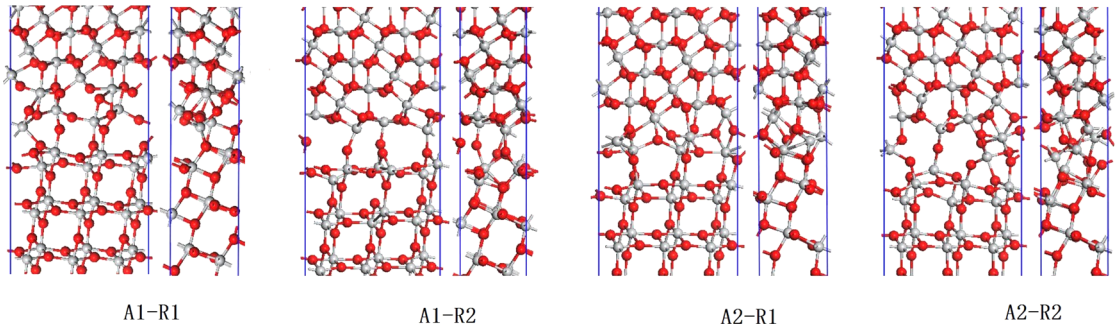

Figure 3. Relaxed interfaces of heterostructures with the interior angle ϕ = 108.7° (front view and side view).

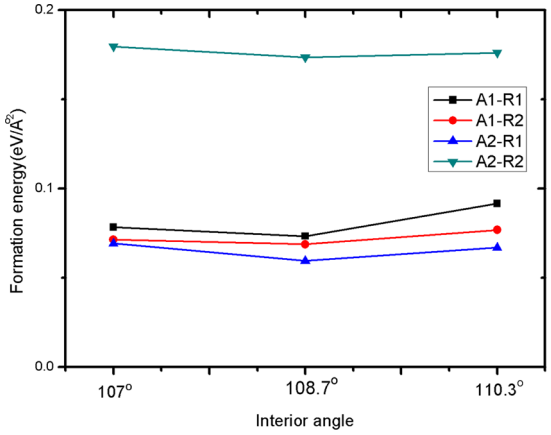

Figure 4. Calculated interfacial formation energies of relaxed heterostructures with different interior angles.

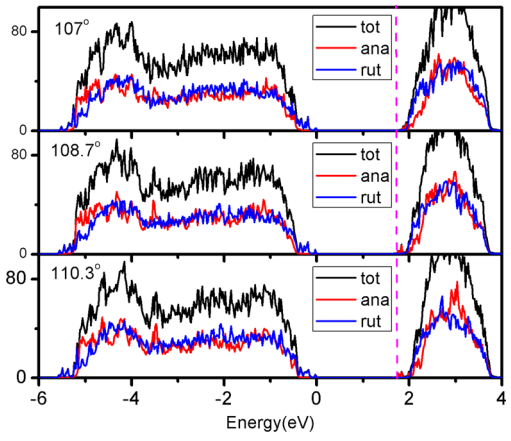

Figure 5. DOS and PDOS of periodic slab model of the heterostructures with different interior angles (ϕ = 107, 108.7, and 110.3°) by PBE.

the lineshapes of valence-band tops of mixed-phase heterostructures are explicitly similar to that of the pure-phase rutile, whereas the conduction-band bottoms are similar to that of the pure-phase anatase. There are a few interesting features in PDOS spectra of the heterostructures. Obviously, the valence-band top of rutile is higher than that of anatase for A2−R1 structures at three different interor angles. This means that the valence-band edges of the heterostructures have the characteristics of the rutile phase component. Meanwhile, we observe that the interior angle has a significant effect on the conduction-band bottoms of A2−R1 heterostructures. At 107°, the conduction-band bottoms of two phases are almost the same. As the interior angle increases, the conduction-band bottom of the anatase phase slightly moves to the lower position at energy levels, whereas that of the rutile phase moves to the higher energy position, leading to that the edges of both the valence and the conduction bands of rutile are higher than those of anatase. The tensile strain around the interface plays a role on the electronic properties of the heterostructures, and it can act as a parameter to tune the band offsets of the heterostructures. To have an accurate band alignment for the heterostructures, we take the most stable structure of A2−R1 with 108.7° as an example to calculate its DOS spectrum and band offsets by the HSE06 functional. Figure 6 shows the calculated total DOS and

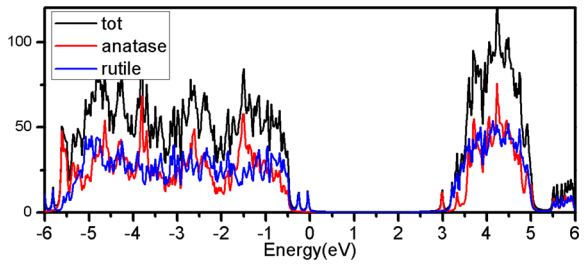

Figure 6. Total DOS and PDOS of periodic slab model of A2−R1 with ϕ = 108.7° by HSE06.

PDOS of this structure. Like the result yielded by PBE, HSE06 also produces the DOS spectrum with its CBM and VBM mainly having the characteristics of anatase and rutile phases, respectively. The calculated band gap of the heterostructure by HSE06 is about 3.0 eV, and those of anatase and rutile phase components are about 3.5 and 3.2 eV, respectively. The slight increasing of around 0.2 eV on the band gaps of both the heterostructure and its two components is due to the quantum-size effect. In order to keep the overall computational cost low, in our interface model, we only contain 5 + 7 layers of surfaces of two phases.

To investigate the effect of the structural reconstruction near the interface on the electronic properties, we calculate the local DOS (LDOS), which is the DOS associated with the atomic layers along the junction, as plotted in Figure 7. Obviously, the band edges are mainly contributed by the atoms located on the layers in a deeper region, not those at the interface. It means that the interface does not yield the defectlike states. In order to visualize these states in the band edges in real space, we extracted the contribution of Kohn−Sham states within the given energy window to form the charge densities. The real-space charge-density distribution are shown in Figure 8. One can see that there is a little charge density localized in the vicinity of the interface. The states that contributed to the tails

dx.doi.org/10.1021/am502830m | ACS Appl. Mater. Interfaces 2014, 6, 12885−12892

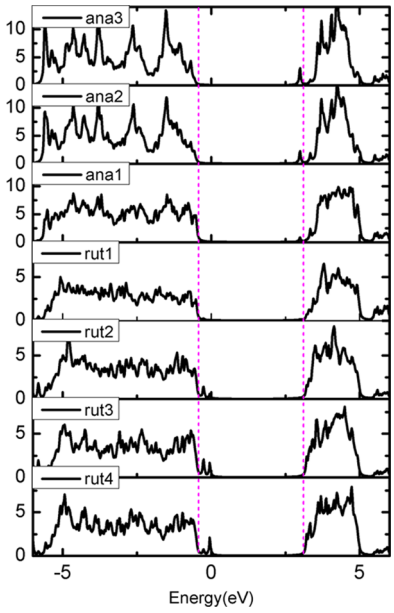

Figure 7. LDOS spectra of the layers around the interface.

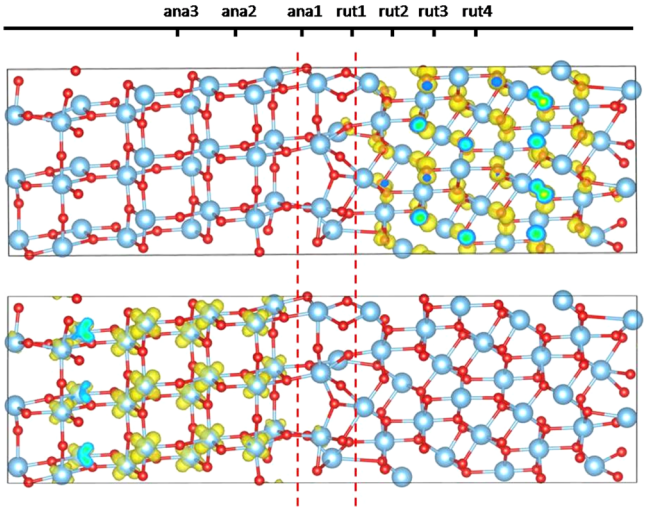

Figure 8. States around the tails of the valence-band top (energy window 0.4 eV) and the conduction-band bottom (energy window 0.15 eV).

of the valence-band top have two dumbbell shapes typical for p orbitals, and these at the conduction-band bottom have four dumbbell shapes typical for d orbitals. It means that the valence-band top has the characteristics of $2p_z$ orbitals of O atoms in the rutile phase and the conduction-band bottom possesses the characteristics of d orbitals of Ti atoms in the anatase phase.

The appearance of tails at the valence-band top of the rutile phase is caused by the stronger overlap between the O $2p_z$ orbitals compared to those in anatase, leading to a substantial splitting of the resulting energy bands, as indicated by Pfeifer et al.[33] The tails appearing at the conduction-band bottom of the total DOS of the heterostructure are all contributed from the d orbitals of Ti in the anatase phase component, which indicates that the d orbitals of Ti in the anatase phase have lower energy than those in the rutile phase. To explain the phenomenon, we display the tetragonal primitive cells of TiO_2 in the anatase and rutile crystal structures in Figure 9. Every Ti atom in the two

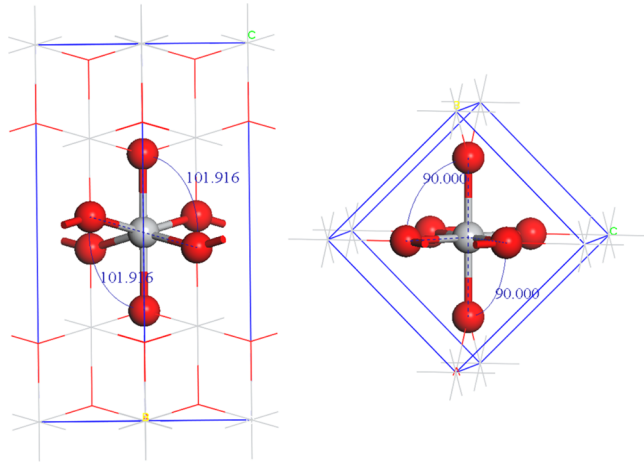

Figure 9. Tetragonal primitive cells of TiO_2 in the anatase and rutile crystal structures.

crystal structures is 6-fold coordinated by oxygens. However, these configurations of the coordinations in the two crystal structures are slightly different. For the rutile crystal structure, there are four oxygens located in the same plane and the other two oxygens are located perpendicular to that plane, whereas, for the anatase crystal structure, two oxygens are bent upward and the other two oxygens are bent downward from the plane, respectively, and the last two oxygens are perpendicular to the plane. The different coordination configurations may affect the energy level of d orbitals of Ti. From Figure 8, the coordination configurations of Ti that belong to the anatase around the interface are changed by relaxation, resulting in the higher energy of d orbitals than that of Ti in a deeper region. We suggest that the coordination configuration in the anatase phase has lower symmetries than that in the rutile phase, resulting in the energy level splitting of the d orbitals of Ti, and some d orbitals of Ti in anatase have lower energy than those in the rutile phase. The tails at the conduction-band bottom are all contributed from the d orbitals of Ti in the anatase phase.

D. Photocatalytic Mechanism of Mixed-Phase Heterostructures. It is well-known that the optical absorption property of a semiconductor photocatalyst, a key factor in determining its photocatalytic activity, is strongly related to its geometrical and electronic structures. We thus calculate the optical absorption spectrum of the mixed-phase TiO_2 by computing the complex dielectric function, and the results are shown in Figure 10. For the comparison, the optical adsorption spectra of two components are also shown. We find that there

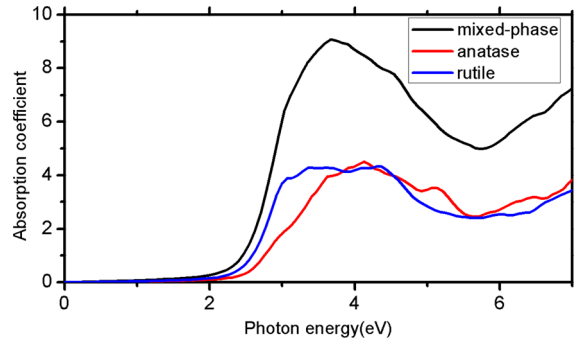

Figure 10. Optical absorption curves of the heterostructure and its two-phase composite particles by PBE.

dx.doi.org/10.1021/am502830m | ACS Appl. Mater. Interfaces 2014, 6, 12885−12892

is no obvious change for the adsorption curve of the heterostructure in comparison with the summation of the adsorption of two components, anatase and rutile, which suggests that the orbital overlap and the electronic transitions between anatase and rutile are negligible, and the direct one-step electronic injection from rutile to anatase seldom takes place by the photoexcitation. The structural reconstruction around the interface thus plays a small role in the light absorption of the heterostructure, and the optical absorption in the heterostructure takes place within anatase and rutile, respectively.

To get an insight into the bonding and charge separation in the vicinity of the interface, we first calculate the difference of the plane-averaged charge (PAC) density of the whole supercell and the sum of PACs of two constituents (individual slabs), obtained after removal of one or the other part. The result shown in Figure 11 manifests that the junction has a quite

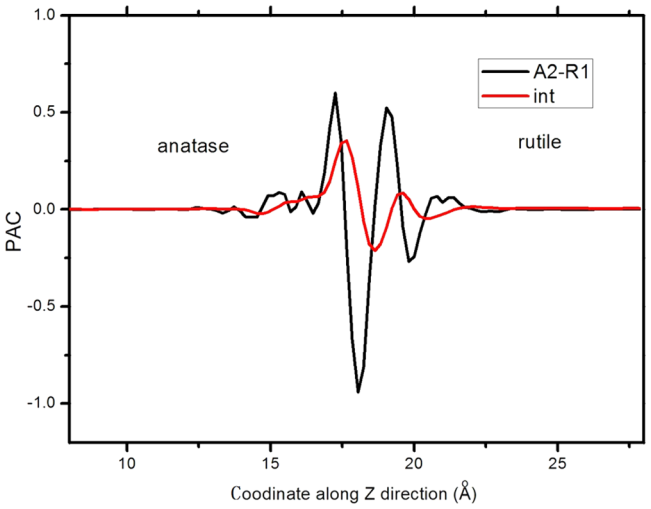

Figure 11. Difference and integral charge transfer of the PAC for A2–R1 with ϕ = 108.7°.

significant charge rearrangement taking place in the vicinity of the interfaces. The charge rearrangement induces the electric field in the junction region. These induced electric fields facilitate the separation and transfer of photogenerated carriers when they diffuse to the junction regions.

To quantitatively assign the band alignment of different phases in the junction according to the intrinsic energy-level alignments of anatase or rutile, we have carried out the separated computational analysis on the mixed-phase junction, and the corresponding anatase and rutile components of the junction. The valence-band offset ΔE_{VBO} can thus be calculated from eq 3 with the values listed in Table 1. As an example, Figure 12a displays the electrostatic potential profile for the mixed-phase junction. It is seen that the built-in potential is localized in the regime with a width of 10 Å, and the potentials out of this regime well represent the properties of the bulk anatase and rutile phases. Figure 12b displays the schematic diagram of the energy-level alignment of the anatase and rutile, and the corresponding VB offsets are 0.52 eV, in agreement with the experimental observation and the previous studies.[33,31] The CB offset is 0.22 eV, which is smaller than that we expected, and the underestimation may be caused by the strain and misfiting of the lattices of two phases. As we analyzed above, the conduction-band bottom is mainly contributed by the d orbitals of Ti of the anatase phases, which is sensitive to the structural configurations. Since both the VB and the CB edges of rutile are higher than those of anatase, the photogenerated electrons upon irradiation of the mixed-phase heterostructure tend to transfer to anatase, whereas the holes transfer to rutile. Meanwhile, the existing electric field in the junction region would hinder electrons and holes to recombine. As a result, the photogenerated electrons and holes can be spatially distributed in two different phases and the charge recombination is inhibited, which is of great benefit for enhancing activity in the photocatalytic reactions.

It is noted that, in the photocatalytic water splitting, the band gap of the photocatalyst is required to be sufficiently large to overcome the character of the water-splitting reaction, and the reduction potential (V_{H^+/H_2} = 4.44 eV)[53] for H^+ to H_2 and the oxidation potential (V_{O_2}/H_2O = 5.67 eV)[53] for H_2O to O_2 should be located inside the band gap. Figure 12b clearly shows that the reduction level is below the CB about 0.35 eV, while the oxidation level is in the gap. This reveals that the oxidation process is energetically favored and the reduction is permitted with a relatively high driving force. Briefly, from the thermodynamic aspect, the junction is a good candidate as photocatalyst for water splitting as the experimental work has indicated.

IV. CONCLUDING REMARKS

We have performed a step-by-step protocol based on the first-principles calculations to investigate the geometrical and electronic properties of mixed-phase TiO_2. Starting from the calculations on DOS spectra of pure-phase anatase and rutile with different DFT XC functionals, we access the accuracy of the DFT XC functional on the electronic structures of bulk materials and find that both PBE and HSE06 can produce the correct relative band gaps of anatase and rutile. However, PBE greatly underestimates the band gaps of bulk TiO_2. HSE06 with α = 0.21 yields the exact band gaps of pure-phase anatase and rutile.

Then, on the basis of an experimental observation, we construct the mixed-phase heterostructures by interfacing the (101) plane of anatase and the (111) plane of rutile. The most stable mixed-phase heterostructures have been identified by the geometrical optimization and the subsequent calculations on the interfacial formation energies. We have also observed that the conduction-band offsets of the heterostructures are

Table 1. Band Gaps for Bulk Anatase and Rutile Phases, the Components for the Calculation of VB and CB Offsets from eq 3, and the Obtained VB and CB Offsets for Mixed-Phase Junction[a]

	E_{ana}^{gap}	E_{rut}^{gap}	$\Delta\bar{V}_{ana-rut}$	$(E_{VBM}-\bar{V})_{rut}$	$(E_{VBM}-\bar{V})_{ana}$	ΔE_{VBO}	$(E_{CBM}-\bar{V})_{rut}$	$(E_{CBM}-\bar{V})_{ana}$	ΔE_{CBO}
HSE06	3.2	3.0	−1.25	10.13	11.9	0.52	14.48	13.01	0.22
PBE	2.0	1.8	−1.45	14.61	12.55	0.61	16.21	14.55	0.21

[a]Units: eV.

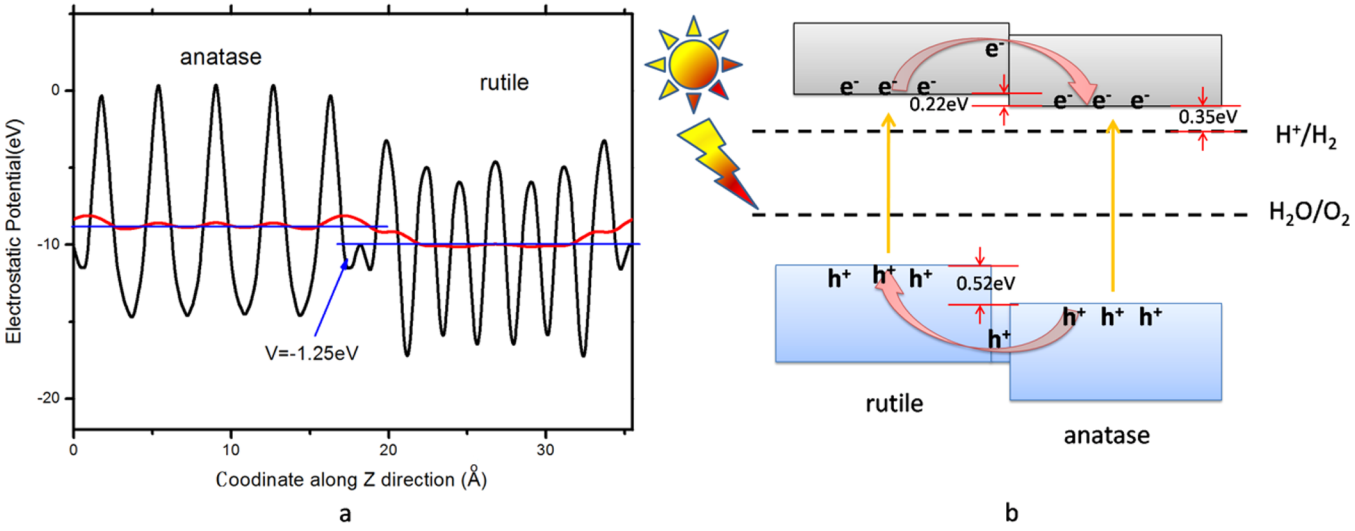

Figure 12. Schematic diagram of electronic potential profile (a), and the band offsets (b).

dependent on the interfacial tensile strain. As the interior angles between two composite structures change, the calculated conduction-band offsets of the heterostructures vary. The tensile strain around the interface plays a role on the electronic properties of the heterostructures, and the strain can act as one of the parameters to tune the band offsets of the heterostructures.

With respect to the hybrid functional HSE06, we calculated the density of states, charge density, optical absorption spectra, and band offsets of the most stable heterostructure. The calculated VBM and CBM of rutile lie 0.52 and 0.22 eV above those of anatase, respectively, which agrees with previous studies by Scanlon et al.,[31] Deák et al.,[34] and Pfeifer et al.[33] The states in the valence-band top and conduction-band bottom have the characteristics of O $2p_z$ orbitals of rutile and Ti d orbitals of anatase, respectively. The lower symmetry of the configurations of 6-fold coordinated Ti atoms in anatase than those in rutile explains why the CB bottom of anatase lies lower in energy than that of rutile. Our calculated band alignment agrees well with experimental measurements and other theoretical predications, and it is favorable for the photogenerated holes in VB to transfer from anatase to rutile and the electrons in CB to transfer from rutile to anatase. The calculated charge depletion layer has a width of about 10 Å around the interface, and the internal field induced in the interface region would further enhance photogenerated charge carrier separation. The good match of band energies to reaction requirements and large driving force for the charge immigration across the interface successfully explain the origin of the high photocatalytic activity achieved by the mixed-phase systems. Meanwhile, we find that the interfacial sites in the mixed-phase TiO_2 have neglecting contributions to light absorption and they also do not dominantly contribute to the states of band edges. The states of band edges are mainly contributed by the atoms in the deep region of the junction, not those near the interfaces, which means that the interfacial sites may not be the loci of the transfer and subsequent trapping of photogenerated charge carriers.

AUTHOR INFORMATION

Corresponding Author

*E-mail: liangwz@xmu.edu.cn.

Notes

The authors declare no competing financial interest.

ACKNOWLEDGMENTS

Financial support from the National Science Foundation of China (Grant No. 21373163 and No. 21290193) and the National Basic Research Program of China (Grant No. 2011CB808501) is acknowledged. The partial numerical calculations have been done on the supercomputing system in the Supercomputing Center of the University of Science and Technology of China.

REFERENCES

(1) Fujishima, A.; Honda, K. Electrochemical Photolysis of Water at a Semiconductor Electrode. *Nature* **1972**, *238*, 37−38.

(2) Mor, G. K.; Shankar, K.; Paulose, M.; Varghese, O. K.; Grimes, C. A. Use of Highly-Ordered TiO_2 Nanotube Arrays in Dye-Sensitized Solar Cells. *Nano Lett.* **2006**, *6*, 215−218.

(3) Sakthivel, S.; Kisch, H. Daylight Photocatalysis by Carbon-Modified Titanium Dioxide. *Angew. Chem., Int. Ed.* **2003**, *42*, 4908−4911.

(4) Parkin, I. P.; Palgrave, R. G. Self-Cleaning Coatings. *J. Mater. Chem.* **2005**, *15*, 1689−1695.

(5) Iuchi, K. I.; Ohko, Y.; Tatsuma, T.; Fujishima, A. Cathode-Separated TiO_2 Photocatalysts Applicable to a Photochromic Device Responsive to Backside Illumination. *Chem. Mater.* **2004**, *16*, 1165−1167.

(6) Wang, J.; Sun, H.; Huang, J.; Li, Q.; Yang, J. Band Structure Tuning of TiO_2 for Enhanced Photoelectrochemical Water Splitting. *J. Phys. Chem. C* **2014**, *118*, 7451−7457.

(7) Dunnill, C. W.; Page, K.; Aiken, Z. A.; Noimark, S.; Hyett, G.; Kafizas, A.; Pratten, J.; Wilson, M.; Parkin, I. P. Nanoparticulate Silver Coated-Titania Thin Films—Photo-oxidative Destruction of Stearic Acid under Different Light Sources and Antimicrobial Effects under Hospital Lighting Conditions. *J. Photochem. Photobiol., A* **2011**, *220*, 113−123.

(8) Gratzel, M. Photoelectrochemical Cells. *Nature* **2001**, *414*, 338−344.

(9) Khan, S. U. M.; Al-Shahry, M.; Ingler, W. B. Efficient Photochemical Water Splitting by a Chemically Modified n-TiO_2. *Science* **2002**, *297*, 2243−2245.

(10) Yang, H. G.; Sun, C. H.; Qiao, S. Z.; Zou, J.; Liu, G.; Smith, S. C.; Cheng, H. M.; Lu, G. Q. Anatase TiO_2 Single Crystals with a Large Percentage of Reactive Facets. *Nature* **2008**, *453*, 638−641.

(11) Akimov, A. V.; Neukirch, A. J.; Prezhdo, O. V. Theoretical Insights into Photoinduced Charge Transfer and Catalysis at Oxide Interfaces. *Chem. Rev.* **2013**, *113*, 4496−4565.
(12) Zhao, J.; Li, B.; Onda, K.; Feng, M.; Peter, H. Solvated Electrons on Metal Oxide Surfaces. *Chem. Rev.* **2006**, *106*, 4402−4427.
(13) Pascual, J.; Camassel, J.; Mathieu, H. Fine Structure in the Intrinsic Absorption Edge of TiO_2. *Phys. Rev. B* **1978**, *18*, 5606−5614.
(14) Tang, H.; Berger, H.; Schmid, P.; Le′vy, F.; Burri, G. Photoluminescence in TiO_2 Anatase Single Crystals. *Solid State Commun.* **1993**, *87*, 847−850.
(15) Riegel, G.; Bolton, J. R. Photocatalytic Efficiency Variability in TiO_2 Particles. *J. Phys. Chem.* **1995**, *99*, 4215.
(16) Hurum, D. C.; Agrios, A. G.; Gray, K. A.; Rajh, T.; Thurnauer, M. C. Explaining the Enhanced Photocatalytic Activity of Degussa P25 Mixed-Phase TiO_2 Using EPR. *J. Phys. Chem. B* **2003**, *107*, 4545−4549.
(17) Hurum, D. C.; Agrios, A. G.; Crist, S. E.; Gray, K. A.; Rajh, T.; Thurnauer, M. C. Probing Reaction Mechanisms in Mixed Phase TiO_2 by EPR. *J. Electron Spectrosc. Relat. Phenom.* **2006**, *150*, 155−163.
(18) Ohno, T.; Sarukawa, K.; Tokieda, K.; Matsumura, M. Morphology of a TiO_2 Photocatalyst (Degussa, P-25) Consisting of Anatase and Rutile Crystalline Phases. *J. Catal.* **2001**, *203*, 82−86.
(19) Ohno, T.; Tokieda, K.; Higashida, S.; Matsumura, M. Synergism between Rutile and Anatase TiO_2 Particles in Photocatalytic Oxidation of Naphthalene. *Appl. Catal., A* **2003**, *244*, 383−391.
(20) Li, G.; Chen, L.; Graham, M. E.; Gray, K. A. A Comparison of Mixed Phase Titania Photocatalysts Prepared by Physical and Chemical Methods: The Importance of the Solid-Solid Interface. *J. Mol. Catal. A: Chem.* **2007**, *275*, 30−35.
(21) Kho, Y. K.; Iwase, A.; Teoh, W. Y.; Madler, L.; Kudo, A.; Amal, R. Photocatalytic H_2 Evolution over TiO_2 Nanoparticles. The Synergistic Effect of Anatase and Rutile. *J. Phys. Chem. C* **2010**, *114*, 2821−2829.
(22) Zhang, J.; Xu, Q.; Feng, Z. C.M.; Li, J.; Li, C. Importance of the Relationship between Surface Phases and Photocatalytic Activity of TiO_2. *Angew. Chem., Int. Ed.* **2008**, *47*, 1766−1769.
(23) Li, G. H.; Gray, K. A. The Solid-Solid Interface: Explaining the High and Unique Photocatalytic Reactivity of TiO_2-Based Nanocomposite Materials. *Chem. Phys.* **2007**, *339*, 173−187.
(24) Qu, Y.; Duan, X. Progress, Challenge and Perspective of Heterogeneous Photocatalysts. *Chem. Soc. Rev.* **2013**, *42*, 2568−2580.
(25) Kawahara, T.; Konishi, Y.; Tada, H.; Tohge, N.; Nishii, J.; Ito, S. A Patterned TiO_2(Anatase)/TiO_2(Rutile) Bilayer-Type Photocatalyst: Effect of the Anatase/Rutile Junction on the Photocatalytic Activity. *Angew. Chem., Int. Ed.* **2002**, *41*, 2811−2813.
(26) Song, K. Y.; Park, M. K.; Kwon, Y. T.; Lee, H. W.; Chung, W. J.; Lee, W. I. Preparation of Transparent Particulate MoO_3/TiO_2 and WO_3/TiO_2 Films and Their Photocatalytic Properties. *Chem. Mater.* **2001**, *13*, 2349−2355.
(27) Kavan, L.; Gratzel, M.; Gilbert, S. E.; Klemenz, C.; Scheel, H. J. Electrochemical and Photoelectrochemical Investigation of Single-Crystal Anatase. *J. Am. Chem. Soc.* **1996**, *118*, 6716−6723.
(28) Miyagi, T.; Kamei, M.; Mitsuhashi, T.; Ishigaki, T.; Yamazaki, A. Charge Separation at the Rutile/Anatase Interface: A Dominant Factor of Photocatalytic Activity. *Chem. Phys. Lett.* **2004**, *390*, 399−402.
(29) Nakajima, H.; Mori, T.; Shen, Q.; Toyoda, T. Photoluminescence Study of Mixtures of Anatase and Rutile TiO_2 Nanoparticles: Influence of Charge Transfer between the Nanoparticles on Their Photoluminescence Excitation Bands. *Chem. Phys. Lett.* **2005**, *409*, 81−84.
(30) Xiong, G.; Shao, R.; Droubay, T. C.; Joly, A. G.; Beck, K. M.; Chambers, S. A.; Hess, W. P. Photoemission Electron Microscopy of TiO_2 Anatase Films Embedded with Rutile Nanocrystals. *Adv. Funct. Mater.* **2007**, *17*, 2133−2138.
(31) Scanlon, D. O.; Dunnill, C. W.; Buckeridge, J.; Shevlin, S. A.; Logsdail, A. J.; Woodley, S. M.; Catlow, C. R. A.; Powell, M. J.; Palgrave, R. G.; Parkin, I. P.; Watson, G. W.; Keal, T. W.; Sherwood, P.; Walsh, A.; Sokol, A. A. Band Alignment of Rutile and Anatase TiO_2. *Nat. Mater.* **2013**, *12*, 798−801.
(32) DiPaola, A.; Bellardita, M.; Ceccato, R.; Palmisano, L.; Parrino, F. Highly Active Photocatalytic TiO_2 Powders Obtained by Thermohydrolysis of $TiCl_4$ in Water. *J. Phys. Chem. C* **2009**, *113*, 15166−15174.
(33) Pfeifer, V.; Erhart, P.; Li, S.; Rachut, K.; Morasch, J.; Brötz, J.; Reckers, P.; Mayer, Y.; Rühle, S.; Zaban, A.; Seró, I. M.; Bisquert, J.; Jaegermann, W.; Klein, A. Energy Band Alignment between Anatase and Rutile TiO_2. *J. Phys. Chem. Lett.* **2013**, *4*, 4182−4187.
(34) Deák, P.; Aradi, B.; Frauenheim, T. Band Lineup and Charge Carrier Separation in Mixed Rutile-Anatase Systems. *J. Phys. Chem. C* **2011**, *115*, 3443−3446.
(35) Wu, C.; Yue, Y.; Deng, X.; Hua, W.; Gao, Z. Investigation on the Synergetic Effect between Anatase and Rutile Nanoparticles in Gas-Phase Photocatalytic Oxidations. *Catal. Today* **2004**, *93*−*95*, 863−869.
(36) Yu, E. T.; McCaldin, J. O.; McGill, T. C. Band Offsets in Semiconductor Heterojunctions. *Solid State Phys.* **1992**, *46*, 1−146.
(37) D'Amico, N. R.; Cantele, G.; Ninno, D. First Principles Calculations of the Band Offset at $SrTiO_3$-TiO_2 Interfaces. *Appl. Phys. Lett.* **2012**, *101*, 141606.
(38) Wang, Z. H.; Zhao, M. W.; Wang, X. P.; Xi, Y.; He, X. J.; Liu, X. G.; Yan, S. S. Hybrid Density Functional Study of Band Alignment in ZnO-GaN and ZnO-$(Ga_{1-x}Zn_x)(N_{1-x}O_x)$-GaN Heterostructures. *Phys. Chem. Chem. Phys.* **2012**, *14*, 15693−15698.
(39) Fan, Y. C.; Zhao, M. W.; He, T.; Wang, Z. H.; Zhang, X.; Xi, Z.; Zhang, H.; Hou, K.; Liu, X.; Xia, Y. Y. Electronic Properties of BN/C Nanotube Heterostructures. *J. Appl. Phys.* **2010**, *107*, 094304.
(40) Fan, Y. C.; Hou, K. Y.; Wang, Z. H.; He, T.; Zhang, X.; Zhang, H.; Dong, J.; Liu, X.; Zhao, M. W. Theoretical Insights into the Built-In Electric Field and Band Offsets of BN/C Heterostructured Zigzag Nanotubes. *J. Phys. D: Appl. Phys.* **2011**, *44*, 095405.
(41) Kresse, G.; Hafner, J. Ab Initio Molecular Dynamics for Liquid Metals. *Phys. Rev. B* **1993**, *47*, 558−561.
(42) Blöchl, P. E. Projector Augmented-Wave Method. *Phys. Rev. B* **1994**, *50*, 17953−17979.
(43) Perdew, J. P.; Burke, K.; Ernzerhof, M. Generalized Gradient Approximation Made Simple. *Phys. Rev. Lett.* **1996**, *77*, 3865−3868.
(44) Heyd, J.; Scuseria, G. E.; Ernzerhof, M. Hybrid Functionals Based on a Screened Coulomb Potential. *J. Chem. Phys.* **2003**, *118*, 8207−8215.
(45) Heyd, J.; Scuseria, G. E. Efficient Hybrid Density Functional Calculations in Solids: Assessment of the Heyd-Scuseria-Ernzerhof Screened Coulomb Hybrid Functional. *J. Chem. Phys.* **2004**, *120*, 7274−7280.
(46) Baldereschi, A.; Baroni, S.; Resta, R. Band Offsets in Lattice-Matched Heterojunctions: A Model and First-Principles Calculations for GaAs/AlAs. *Phys. Rev. Lett.* **1988**, *61*, 734−737.
(47) Conesa, J. C. Modeling with Hybrid Density Functional Theory the Electronic Band Alignment at the Zinc Oxide-Anatase Interface. *J. Phys. Chem. C* **2012**, *116*, 18884−18890.
(48) Zhang, X. .R; Lin, Y. H.; He, D. Q.; Zhang, J. F.; Fan, Z. Y.; Xie, T. F. Interface Junction at Anatase/Rutile in Mixed-Phase TiO_2: Formation and Photo-Generated Charge Carriers Properties. *Chem. Phys. Lett.* **2011**, *504*, 71−75.
(49) Popov, M. N.; Spitaler, J.; Mühlbacher, M.; Walter, C.; Keckes, J.; Mitterer, C.; Draxl, C. $TiO_2(100)/Al_2O_3(0001)$ Interface: A First Principles Study Supported by Experiment. *Phys. Rev. B* **2012**, *86*, 205309−205322.
(50) Zhang, S. B.; Northrup, J. E. Chemical Potential Dependence of Defect Formation Energies in GaAs: Application to Ga Self-Diffusion. *Phys. Rev. Lett.* **1991**, *67*, 2339−2342.
(51) Finnis, M. W.; Lozovoi, A. Y.; Alavi, A. THE OXIDATION OF NiAl: What Can We Learn from Ab Initio Calculations? *Annu. Rev. Mater. Res.* **2005**, *35*, 167−207.
(52) Wang, W. C.; Chen, S. Y.; Yang, P. X.; Duan, C. G.; Wang, L. W. Si:WO_3 Heterostructure for Z-Scheme Water Splitting: An ab Initio Study. *J. Mater. Chem. A* **2013**, *1*, 1078−1085.
(53) Li, X. X.; Zhao, J.; Yang, J. L. Semihydrogenated BN Sheet: A Promising Visible-Light Driven Photocatalyst for Water Splitting. *Sci. Rep.* **2013**, *3*, 1858−1863.